Twelfth Australasian Fluid Mechanics Conference
The University of Sydney, Australia 1995

COMPUTATIONAL SIMULATIONS OF PULSATING TURBULENT PIPE FLOW

J. D. Jackson and Shuisheng He
Manchester School of Engineering
University of Manchester
Manchester M13 9PL
The United Kingdom

ABSTRACT

Results from experiments on pulsating turbulent pipe flow are compared with computational simulations made using the low-Reynolds number k-ε turbulence models of Launder and Sharma, Lam and Bremhorst and Shih and Hsu. The LS and LB simulations generally predict the correct response of the mean flow and the turbulence. The SH simulations were less successful in reproducing observed behaviour, particularly in the case of turbulent shear stress.

1. INTRODUCTION

In this paper, we report direct comparisons between some experiments on pulsating turbulent pipe flow and computational simulations made using three low-Reynolds number k-ε turbulence models. Over the years, the development of such models has received intensive study and a variety of formulations have been proposed. They have mainly been validated by comparison with experiments for a few widely-studied steady flow situations. Recently, the present authors have reported direct comparisons between their experiments on transient turbulent pipe flow with imposed excursions of flow rate of ramp-type (Jackson and He 1993) and simulations using a variety of turbulence models (Jackson and He 1995). In particular, the performance of the models was critically evaluated in terms of their ability to capture certain important features of ramp-type transient flow involving delays in the response of turbulence as well as in terms of general agreement with data. The present authors have subsequently undertaken experiments on pulsating turbulent pipe flow (Jackson and He 1994). These have yielded new and useful results which provide further scope for evaluating turbulence models. Careful planning of the experiments led to a more comprehensive coverage of experimental conditions being made than hitherto.

2. EXPERIMENTAL DETAILS

The experiments were carried out with fully developed flow of water using a long pipe of internal diameter 50.4 mm. A very repeatable sinusoidal variation of flow rate with time about a steady mean level was achieved using a computer-controlled, pneumatically-actuated valve. A counter/timer module used in conjunction with a turbine flowmeter enabled measurements of instantaneous flow rate to be made with high accuracy. A two-component laser Doppler anemometer system enabled simultaneous measurements of the axial and radial components of the instantaneous velocity field to be made. The strategy of data reduction used was basically one of ensemble averaging the results of numerous successive experiments in which the same variation of flow rate was imposed with great repeatability. In the majority of the experiments, the Reynolds number based on the mean values of the flow rate was 7000 and the amplitude (peak to mean) was 20%. The time period of pulsation was systematically varied from 2 to 20 seconds to cover a range of non-dimensional time period τ_R(=2/3 $U_\tau T/R$) from 0.47 to 4.7. The parameter τ_R is the ratio of the time period of the imposed flow pulsation to the time scale for the propagation of turbulence radially from the near wall region of the flow to the centre. Turbulence can be thought of as starting to freeze in the core region when the parameter τ_R is less than unity. Experiments with higher values of mean Reynolds number (10500 and 14000) or higher values of peak to mean flow rate (47%) were also conducted.

3. THE TURBULENCE MODELS AND NUMERICAL METHOD

Three representative low-Reynolds number k-ε turbulence models were chosen for examination in the present study. These include the pioneering model of this kind due to Launder and Sharma (1974) and the variant proposed later by Lam and Bremhorst (1981). The third model examined is a recent one due to Shih and Hsu (1991), which has been developed using DNS data.

The equations for the transport of k and ε can be written in a general form as:

$$\frac{\partial k}{\partial t}=\nu_t\left(\frac{\partial U}{\partial r}\right)^2+\frac{1}{r}\frac{\partial}{\partial r}\left[r\left(\nu+\frac{\nu_t}{\sigma_k}\right)\frac{\partial k}{\partial r}\right]-\varepsilon+\Pi \qquad (1)$$

$$\frac{\partial \varepsilon}{\partial t}=\frac{1}{r}\frac{\partial}{\partial r}\left[r\left(\nu+\frac{\nu_t}{\sigma_\varepsilon}\right)\frac{\partial \varepsilon}{\partial r}\right]+C_{\varepsilon 1}f_1\frac{\varepsilon}{k}\nu_t\left(\frac{\partial U}{\partial r}\right)^2-C_{\varepsilon 2}f_2\frac{\varepsilon^2}{k}+E \qquad (2)$$

The model constants and damping functions are given in Tables 1 to 4 along with other details.

The computer code used was specifically developed in the course of the present study for modelling transient

Table 1. Model Constants

Model	C_μ	C_1	C_2	σ_k	σ_ε
LS	0.09	1.44	1.92	1.0	1.3
LB	0.09	1.44	1.92	1.0	1.3
SH	0.09	1.5	2.0	1.3	1.3

Table 2. Damping Functions

Model	f_μ	f_2
LS	$\exp\left(\frac{-3.5}{(1+Re_t/50)^2}\right)$	$1-0.3\exp(-Re_t^2)$
LB	$[1-\exp(-0.0165Re_y)]^2\left(1+\frac{20.5}{Re_t}\right)$	$1-\exp(-Re_t^2)$
SH	$1-\exp(-a_1Re_u^{1/4}-a_2Re_u^{1/2}-a_3Re_u)$ *where* $a_1=5e-3,\ a_2=7e-5,\ a_3=8e-7$	$\left[1-0.22\exp(-\frac{Re_t^2}{36})\right]\frac{\tilde{\varepsilon}}{\varepsilon}$
Note: $f_1=f_3=1$ in all the models except $f_1=1+(0.05/f_\mu)^3$ in LB		

Table 3. Extra Terms

Model	D	E
LS	$2\nu(\partial\sqrt{k}/\partial y)^2$	$2\nu\nu_t(\partial^2U/\partial y^2)^2$
LB	0	0
SH	$\varepsilon\exp(-Re_t^{1/2})$	$2\nu\nu_t(\partial^2U/\partial y^2)^2$
Note: $\Pi=0$ in all the models except that in SH $\Pi=\frac{1}{r}\frac{\partial}{\partial y}\left(r\frac{0.01}{f_\mu^2}\frac{\nu_t}{\sigma_k}\frac{\partial k}{\partial y}\right)$		

Table 4. Model Features

Model	Dissipation Equation	B. C. of ε_w	Length Scale	Asymptotic feature of ν_t	Parameters used in f_μ	Behaviour of f_μ	ε near wall	Other features
LS	$\tilde{\varepsilon}$	$\tilde{\varepsilon}_w=0$	$k^{3/2}/\tilde{\varepsilon}$	$0(y^3)$	Re_t	Too fast at first & too slow later		
LB	ε	$\partial\varepsilon/\partial y=0$ *or* $\varepsilon_w=\frac{\nu\partial^2k}{\partial y^2}$	$k^{3/2}/\varepsilon$	$0(y^4)$	Re_y & Re_t	Slightly too slow later		
SH	ε	$\varepsilon=2\nu(\partial\sqrt{k}/\partial y)^2$	$k^{3/2}/\tilde{\varepsilon}$	$0(y^3)$	Re_U	Fine	Reaches a maximum	Accounting for pressure diffusion
Note: $\nu_t=C_\mu f_\mu\frac{k^2}{\varepsilon}$, $\tilde{\varepsilon}=\varepsilon-D$, $Re_t=\frac{k^2}{\nu\varepsilon}$, $Re_y=\frac{\sqrt{k}y^+}{\nu}$, $y^+=\frac{u_\tau y}{\nu}$ and $Re_U=\frac{U^4}{\nu\varepsilon}$								

turbulent pipe flow using Fortran on HP workstations. A finite volume/finite difference scheme is used and the calculation is of explicit marching type in time.

4. RESULTS

4.1 Experiments with 3, 6 ,10 and 20 second transients and LS model simulations

Figure 1 shows measured radial distributions of the amplitude of velocity modulation in pulsating flows with various flow pulsation time periods. The time-mean Reynolds number and amplitude of flow pulsation are fixed. Also shown in the figure are the corresponding results from simulations performed using the LS model. The experimental results show that the variation of amplitude of velocity modulation exhibits interesting non-monotonic changes as the time period is varied. In the core region, the amplitude of velocity modulation first decreases with the reduction of time period and then for T < 6s it increases. With higher frequency of pulsation, the flow in the core region exhibits a slug-like behaviour. As the frequency is reduced, the extent of this region reduces and the behaviour disappears for time periods of 6 seconds and above. The amplitude of velocity modulation reaches a maximum at a location which shifts towards the centre of the pipe with the increase of the time period. These features are in fact similar to those found in laminar pulsating flows but the time scales involved and some details of the variation are different. As can be seen from Figure 1, all the features of the experimental results identified above are reproduced by the simulations. They are in particularly good agreement with the experimental data for the cases of the 3 and 6 second transients. Although the agreement is less close in the case of the slower transients, the trends are still clearly predicted.

Figure 2 shows the time delay of the ensemble averaged velocity relative to the mean flow in experiments with fixed time mean Reynolds number and peak to mean amplitude of flow pulsation. Also shown are the corresponding results from simulations using the LS model. The experimental results clearly show that in the faster transients the time delay, or phase shift, in the core region is close to zero (the pulsation being locked to the mean flow). With the increase of time period, the extent of the region where the phase shift is zero reduces and it disappears in the transients of 6 second period and greater. It is can be seen that the location of the maximum delay in the 3 second transient is near to the wall and it moves away from the wall with the increase of the time period of the transient. This location shifts to the centre of the pipe in the slower transients. The numerical simulations generally reproduce the general trends quite well over the entire range of frequency. Quantitatively, the predictions for the slower transients are not in as good agreement with the data as those for the faster ones. It is worth noting that both the numerical and experimental results show that the distributions of the time delay of velocity follow a very

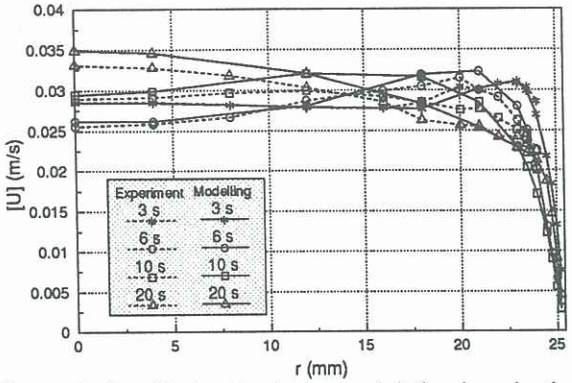

Figure 1 Amplitude of velocity modulation in pulsating flows with various time periods - comparison between experiment and the LS model simulations

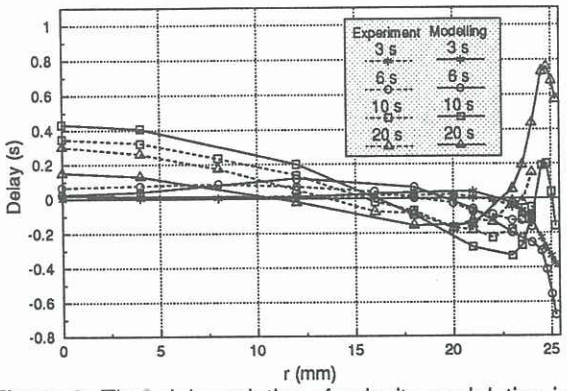

Figure 2 Time delay relative of velocity modulation in pulsating flows with various time periods - comparison between experiment and the LS model simulations

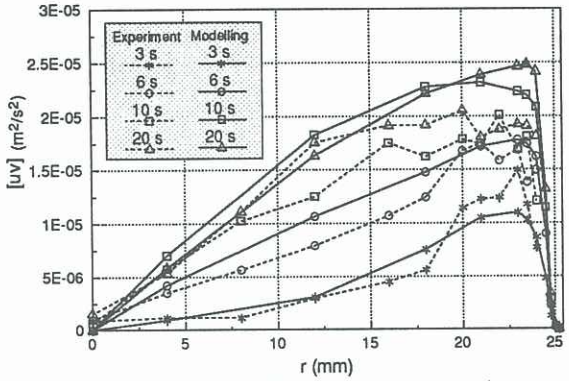

Figure 3 Amplitude of turbulent shear stress in pulsating flows with various time periods - comparison between experiment and the LS model simulations

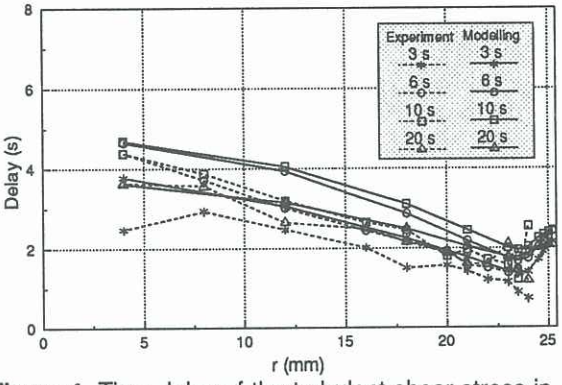

Figure 4 Time delay of the turbulent shear stress in pulsating flow with various time periods - comparison between experiment and the LS model simulations

different pattern from the rest in the case of the 10 and 20 second transients. The location of the minimum delay shifts away from the wall. It is of interest to note that the numerical predictions show that the delay peaks a second time at a location close to the wall (no experimental data are available in that region).

Figure 3 shows the radial distributions of the amplitude of modulation of the mean product of the radial and axial components of the turbulent fluctuations (the turbulent stress) for various time periods. When the frequency of flow pulsation is low (the 10 and 20 second time period cases), the variations of the amplitude of the uv with time period are very similar to those obtained in the case of pseudo-steady flows. However, with decrease of the time period of flow pulsation, the amplitude is reduced. In the extreme case of a 3 second transient, the amplitude becomes almost zero over a significant part of the core region of the flow. The turbulence is frozen in that region. The numerical predictions again capture the general trends exhibited by the experimental data, although some quantitative discrepancies can be seen. These can be attributed partly to experimental uncertainty.

Figure 4 shows the time delay of the modulations of turbulent shear stress relative to the imposed flow pulsation in experiments with various time periods. It can be seen that the time delay increases with the distance from the wall over most of the flow. The absolute delay time is very similar in the 6 and 10 second flow transients. It is slightly lower in the 20 second transient and significantly lower in the 3 second one. Whereas the general patten of the variation of the delay with radial position is captured fairly well, there are clear quantitative discrepancies between the numerical predictions of time delay and the experimental values. The dependency on frequency of the delay is captured quite well: the delay predicted is similar in the 6 and 10 second flow transients and is lower in the 3 and 20 second cases. The near wall variations of time delay obtained from the predictions (not available from the experiment) show that the smallest delay occurs at a location within a small distance from the wall and the delay builds up in both directions on moving away from this location.

4.2 Comparison of simulations using the various models for the case of a 6 second transient

Figures 5 and 6 show the radial distribution of the amplitude and time delay, relative to the imposed flow, of the velocity modulation for a pulsating flow with a 6 second time period. In each case, simulations using the three turbulence models are presented along with the experimental results on the same figure. It can be seen that, in terms of the radial distribution of amplitude, the LS model gives results closest to the experimental data with the LB model performing next best. The simulation

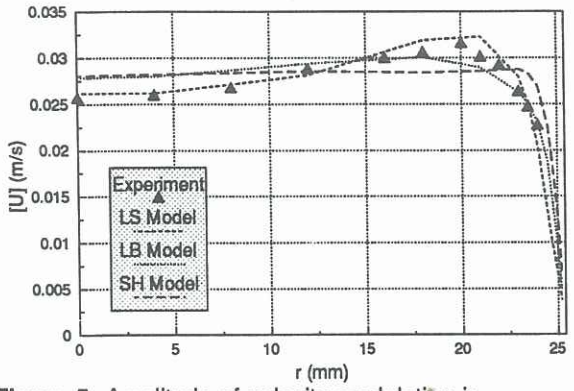

Figure 5 Amplitude of velocity modulation in pulsating flow with a 6 second time period

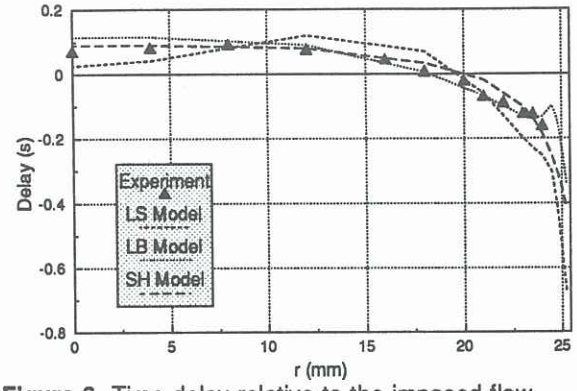

Figure 6 Time delay relative to the imposed flow of velocity modulation in pulsating flow with a 6 second time period

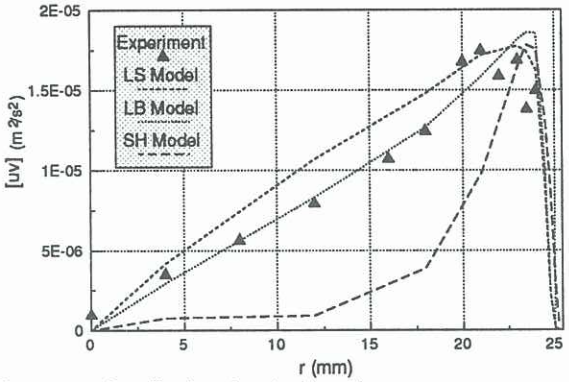

Figure 7 Amplitude of turbulent shear stress in pulsating flow with a 6 second time period

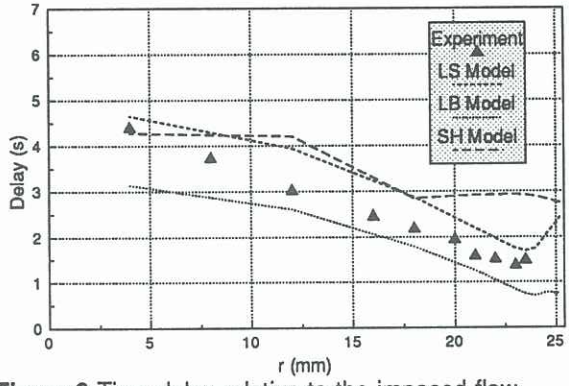

Figure 8 Time delay relative to the imposed flow of turbulent shear stress in pulsating flow with a 6 second time period

using the SH model is less satisfactory. Its results show features that we have seen earlier with faster transient flows. The amplitude does not vary much in the core region of the flow and peaks at a position which is close to the wall. In terms of time delay, the predictions of both the LB and SH models are slightly better than those of the LS model.

Figures 7 and 8 show both the simulations and experimental results for amplitude and the time delay of the turbulent shear stress. The simulations yielded by the LS and LB models lie fairly close to the experimental points. However, the SH model gives results which are quite different. It wrongly predicts that the response of the turbulent shear stress is effectively frozen in the core.

4. CONCLUSIONS

The present simulations of pulsating flow made using the LS and LB models generally predicted the correct response of both the mean flow and the turbulence. The predictions of amplitude were closer to the experiment than those of time delay. The two models performed equally well in the comparative study carried out here. The SH model was less successful in reproducing observed behaviour, particularly in the case of turbulent shear stress. Some interesting information concerning the near wall response of the flow and turbulence has been yielded by the simulations.

REFERENCES

J.D. Jackson and S. He (1995) 'Simulations of transient turbulent flow using various two-equation low-Reynolds Number turbulence model', Presented at the 10th Symposium Turbulent Shear Flows, The Pennsylvania State University, PA, USA, Aug. 14-16 1995.

J.D. Jackson and S. He (1994) 'An experimental study of pulsating turbulent pipe flow', Proceedings of Int. Sym. on Turbulence, Heat and Mass Transfer, Lisbon, Portugal, Aug. 9-12, 1994.

J.D. Jackson and S. He (1993) 'Turbulence propagation in transient turbulent shear flows', in Near-Wall Turbulent Flows (Eds. R.M.C So, C.G. Speziale and B.E. Launder), pp939-948, Elsevier.

Lam, C.K.G. and Bremhorst, K. (1981) 'A modified form of the k-ε model for predicting wall turbulence' ASME Transactions, Journal of Fluids Engineering, Vol.103, pp456-460.

Launder, B.E. and Sharma, B.I. (1974) 'Application of energy dissipation model of turbulence to the calculation of flow near a spinning disc' Let. Heat Mass Transfer, Vol. 1, pp131-138.

Shih, T.H. and Hsu, A.T. (1991) 'An improved k-ε model for near-wall turbulence' AIAA Paper, AIAA-91-0611.